Electronic structure of the dilute magnetic semiconductor $Zn_{0.90}Mn_{0.10}S$ obtained by soft x-ray spectroscopy and first-principles calculations

T. M. Schuler, R. A. Stern,* R. McNorton, S. D. Willoughby,† J. M. MacLaren, and D. L. Ederer
Department of Physics, Tulane University, New Orleans, Louisiana 70118, USA

V. Perez-Dieste and F. J. Himpsel
Department of Physics, University of Wisconsin-Madison, Madison, Wisconsin 53706, USA

S. A. Lopez-Rivera
Laboratorio de Fisica Aplicada, Universidad de los Andes, Merida, Venezuela

T. A. Callcott
Physics and Astronomy Department, University of Tennessee, Knoxville, Tennessee 37996, USA
(Received 10 May 2004; revised manuscript received 17 May 2005; published 18 July 2005)

Soft x-ray emission and absorption spectra of the Mn $L_{2,3}$-edge were obtained from the diluted magnetic semiconductor $Zn_{0.90}Mn_{0.10}S$, and interpreted with the aid of first-principles computations of the densities of states. The calculations reveal that the Mn *d* states near the Fermi energy show interesting spin polarization, and are strongly hybridized with the neighboring S atoms, indicative of the *sp-d* hybridization typical of dilute magnetic semiconductors. Resonant inelastic x-ray measurements reveal a 3-eV inelastic energy loss, which is interpreted as a transition from the Mn valence-band *d* states to a spin-flip multiplet of the $3d^5$ ground-state configuration, while a 6-eV loss is attributed to observed charge-transfer effects caused by hybridization between the S *p* states and the occupied Mn *d* states located a few eV below the Fermi energy.

DOI: 10.1103/PhysRevB.72.045211 PACS number(s): 71.55.Gs, 75.50.Pp, 78.70.Dm, 78.70.En

INTRODUCTION

Semiconductors containing small amounts of magnetic impurities, also known as dilute magnetic semiconductors (DMS's), have been of interest to the physics and engineering communities for quite some time.[1–4] Recently, room-temperature ferromagnetism has been observed in DMS systems,[5] intensifying efforts to merge traditional electronics with magnetoelectronics, whereby spins are switched instead of, or in addition to, charges, allowing control over a semiconductor device with a magnetic field.

The presence of magnetic ions in a semiconductor host leads to spin-spin exchange interactions between localized magnetic moments and valence-band electrons, as well as between the magnetic ions themselves. These strong magnetic interactions are due to the presence of localized magnetic moments, which arise from the partially filled electronic shells of transition-metal ions introduced into the host as dopants.[6] These interactions affect the energy band and impurity level parameters of the semiconductor, resulting in interesting physical effects such as an extremely large Faraday rotation (on the order of 1000°/cm kG at low temperatures),[3] large Zeeman splitting of the free exciton (on the order of 100 meV or more),[7] giant negative magnetoresistance associated with electrons hopping in the conduction band, and the bound magnetic polarons.[4] The large Faraday effect is a direct consequence of the electron-magnetic ion exchange interaction, which induces a large spin splitting of the electronic states in an applied magnetic field with corresponding *g*-factors on the order of 100.[6] This has led to consideration of these materials for use in magneto-optical isolators to protect semiconductor lasers from reflected noise, especially at wavelengths of interest for optical fiber systems.[8]

DMS's are also disordered magnetic alloys, which produce a frustrated spin-glass state at low temperatures when accompanied by antiferromagnetic coupling between magnetic ions (as is often the case for Mn impurities).[4] Furthermore, the semiconducting properties of DMS's, such as the band gap, effective mass, etc., can be varied in a controlled fashion by varying the composition, much as in nonmagnetic ternary semiconductors.[4,9] The DMS most widely studied has been Mn in GaAs, where Curie temperatures of 110 K have been achieved[1] and higher Curie temperatures might be possible under special growth conditions. For such systems a fairly detailed picture exists of the interaction between the magnetic impurity and the host. Mn substitutes for Ga in a mixture of the Mn^{2+} and Mn^{3+} oxidation states, and the 3*d* electron count is slightly more than 5.[10] Although the main concentration of occupied Mn 3*d* states lie 2–4 eV below the Fermi energy ($\boldsymbol{E_F}$),[11–13] with only a small number of states located at $\boldsymbol{E_F}$, they are able to affect the carriers in the GaAs host by spin-polarizing holes near the As 4*p*-derived valence-band maximum.[10] The interaction is antiferromagnetic and very efficient, resulting in very large *g*-factors, given that a single Mn impurity can polarize many carriers. The unoccupied Mn 3*d* states have been found to lie 3.9 eV above the Fermi edge by inverse photoemission,[14] leading to a substantial ferromagnetic exchange splitting of 4.31 eV for the Mn 3*d* states. This is consistent with a large magnetic moment approaching the $5\mu_B$ atomic limit, according to an empirical rule of about 1 eV splitting per Bohr magneton,[15]

as well as recent calculations for magnetically doped ZnS systems.[16]

In an effort to raise Curie temperatures to values above room temperature, a point at which magnetic semiconductors could become commercially viable, interest has shifted to hosts with larger band gaps, such as GaP and ZnO which have gaps of 2.3 eV (Ref. 17) and 3.4 eV (Ref. 18), respectively. ZnS has a comparable gap of 3.68 eV, prompting research into the electronic structure of Mn in ZnS and other II-VI DMS's.[3] The tunability of electronic parameters in DMS's has led to the use of II-VI DMS in the construction of ZnSe-based semiconductor lasers operating in the blue-green region of the spectrum.[19] Like other DMS's, II-VI compounds show novel magneto-optical and magnetotransport properties when the cation is partially substituted by Mn; in bulk $Cd_{1-x}Mn_xTe$, the Faraday rotation values on the order of 10^5 deg/T cm.[6]

Experimental studies have provided a wealth of information on the electronic structure and properties of II-IV DMS's. In $Ga_{1-x}Mn_xAs$, empty $3d$ states have been probed with soft x-ray absorption spectroscopy (XAS) by exciting electrons from the Mn $2p_{3/2,1/2}$ core levels at 640 and 651 eV below the Fermi energy.[20] Previously reported x-ray spectroscopy measurements have suggested that occupied Mn $3d$ impurity states are localized 2–3 eV below the valence-band edge in a doped ZnS:Mn compound.[12] Synchrotron based photoemission spectra concerning the valence electron states of the series $Zn_{1-x}Mn_xY$, where Y=S, Se, and Te, have also been reported, which support the observations that the $3d$ impurity states are localized 3–4 eV below the valence-band edge and that the strongest hybridization occurs with an Mn impurity in ZnS.[13] From a Raman study of $Zn_{1-x}Mn_xS$ and $Zn_{1-x}Fe_xS$ in the visible spectral range, it has been determined that hybridization is a factor in these systems due to a large "breathing mode" associated with the defect's nearest-neighbor S atoms.[21] Measurements of the low-temperature heat capacity of II-VI DMS's have led to the determination that the magnetic ions interact with each other out to the fourth nearest neighbor, although the coupling beyond the nearest neighbor is small, on the order of 0.3 K (25 μeV).[22] Optical measurements in the presence of a magnetic field reveal a transition in the vicinity of 2.2 eV emphasizing the localized nature of the Mn^{2+} levels with focus on ligand fields. The 2.2-eV feature of Mn^{2+} is attributed to a transition from the $^6A_1(^6S)$ symmetric ground state of the $3d^5$ configuration to the lowest crystal-field split $^4T_1$ component of the first excited state (^4G) in which one of the $3d^5$ electrons has antiparallel spin.[7]

In this paper we report results from x-ray spectroscopic measurements performed on $Zn_{0.90}Mn_{0.10}S$, in which the occupied valence Mn bands and the unoccupied conduction Mn bands were observed and even parity electron transitions are mapped, including a 3-eV Raman transition corresponding to the above-mentioned spin-flip transition consistent with an atomic model[23,24] and a 6-eV charge-transfer transition, with support for the interpretation of these transitions from our calculations. We also report first principles DFT calculations on a system with a transition-metal impurity in ZnS which shows the partial density of states (PDOS) having "d" symmetry as localized with respect to the nearest-neighbor S atoms. Our x-ray emission and absorption measurements suggest a significant level of hybridization throughout the valence and conduction bands, although it is shown to be most prevalent between Mn d states and S p states within the valence band. Used in conjunction with the calculated densities of states we can assume that Mn and S atoms play a majority role in the bonding of the Mn atoms when a ZnS sample is doped to create a diluted magnetic semiconductor.

EXPERIMENT

With the evolution of high intensity synchrotron light sources and efficient detectors, the photon-in/photon-out processes of x-ray-absorption spectroscopy (XAS) and x-ray emission spectroscopy (XES) have become useful tools for examining the electronic bonding in solids. This is primarily because XAS and XES can give site- and element-specific information about both the valence and conduction bands of compound systems.

X-ray absorption involves the photon excitation of a core-level electron into the conduction band of the material, mapping the states located above the Fermi edge. The process of x-ray emission occurs when an electron descends from a higher energy state to fill a core hole left by an absorption process, releasing a photon in the process. By tuning the excitation energy to specific absorption energies we can measure the photons emitted by both resonant elastic and resonant inelastic scattering processes, providing detailed information about the valence and core electron states of the system.

The experimental measurements reported here were performed on crystalline samples of $Zn_{0.90}Mn_{0.10}S$. Details on sample preparation have been published elsewhere.[21] The Mn concentration yields a doping level within the range of approximately $2.5–5.1\times10^{21}$ Mn atoms per cubic cm. Although general approximations of the crystal structures of II-VI DMS's suggest that a ZnS sample doped with Mn atoms at a concentration of 10% or less should have zinc-blende (sphalerite) structure,[3] our experimental sample has been verified via x-ray diffraction (XRD) measurements[25] as having wurtzite crystal structure. The lattice constant used in the calculation follow the trend derived for different doping levels, which gives the mean cation-cation distance (d_c) for $Zn_{1-x}Mn_xS$ as[26]

$$d_c(Zn_{1-x}Mn_xS) = (3.8300 \pm 0.0005) + (0.1391 \pm 0.0010)x \quad (1)$$

providing d_c=3.843 Å for x=0.10. The lattice parameters a and c for a wurtzite crystal are then obtained from the relations[3]

$$a = d_c, \quad c = \left(\frac{8}{3}\right)^{1/2} d_c \quad (2)$$

yielding a=3.843 Å and c=6.276 Å for our sample. The Mn atoms are introduced substitutionally onto the Zn sites, as has been observed in nanocrystals.[27]

The XAS and XES measurements were made at Beamline 8.0.1 of the Advanced Light Source located at Lawrence

Berkeley National Laboratory, which is an undulator beamline equipped with a spherical grating monochromator as described by Jia *et al.*[28] The XES and XAS experimental configuration consists of monochromatized soft x-rays with linear polarization directed onto a sample at an incident angle of 45° in order to generate core electron excitations. A pico-ammeter was connected to the sample plate in order to detect the current through the sample and measure the total electron yield (TEY). The photons that fluoresced from the sample were either collected by a channeltron biased to reject electrons to measure the partial fluorescence yield (PFY), or were passed into the spectrometer chamber (XES), where a spherical grating diffracted them to a multichannel detector positioned along the Rowland circle set to obtain the desired energy range. The spectral intensity was normalized relative to the intensity of the incident radiation, which is derived from the emitted current of a gold mesh placed in the beam path. The incident and emitted photon energies were calibrated to within an accuracy of 0.5 eV by comparison of measurements of an Mn metal reference sample to accepted, previously published absorption and emission energy values.[29]

CALCULATIONS

The electronic structures of stoichiometric ZnS zinc-blende and Mn-doped ZnS wurtzite crystals were calculated using first-principles density-functional theory (DFT) techniques.[30] The software used was the well-known Vienna Ab-initio Simulation Package (VASP),[31] using projector augmented wave (PAW) potentials.[32,33] Exchange and correlation energies were treated within the generalized gradient approximation (GGA),[34] using the functional of Perdew-Wang 1991 (PW91),[35] along with the interpolation of Vosko, Wilk, and Nusair.[36] Site-, spin-, and angular momentum-resolved densities of states (DOS) as well as the exchange coupling between Mn defects were calculated.

Imitating previous DFT calculations for transition metal impurities in ZnS,[16] we simulated an Mn defect in a wurtzite matrix by constructing a supercell containing eight formula units (16 atoms), with a single Zn atom replaced by an Mn atom. This material $Zn_{7/8}Mn_{1/8}S = Zn_{0.875}Mn_{0.125}S$ is reasonably similar to the experimental sample $Zn_{0.90}Mn_{0.10}S$; in both cases the dilute limit holds. The experimental lattice constant of 5.41 Å was used for stoichiometric ZnS calculations and the derived lattice constants [from Eqs. (1) and (2)] for Zn_7MnS_8 were found to be $a=3.847$ Å and $c=6.283$ Å. The Mn potential treated the $3p$ semicore states as valence states, and energy cutoffs of 24.3 and 26.5 Ry were used in the ZnS and Zn_7MnS_8 computations, respectively. For DOS calculations with supercells containing one defect Mn atom, integrations in the Brillouin zone were performed on a $5\times5\times3$ mesh with a total of 24 k-points, while for the exchange calculations, which require supercells twice as big containing two defect Mn atoms, a $3\times3\times1$ grid for a total of 4 k-points was used to reduce calculation time while still maintaining a total-energy convergence of better than 1.0 meV/atom for all calculations.

Exchange calculations were also performed using two 16 atom supercells and varying the separation distances between the two Mn atoms for a comparison of exchange vs the separation distance. For all of the Mn-Mn separation distances calculated, the exchange energies suggested antiferromagnetic ordering with a low Curie temperature (~3.5 K), but were unable to determine a most likely Mn-Mn separation distance with any numerical significance.

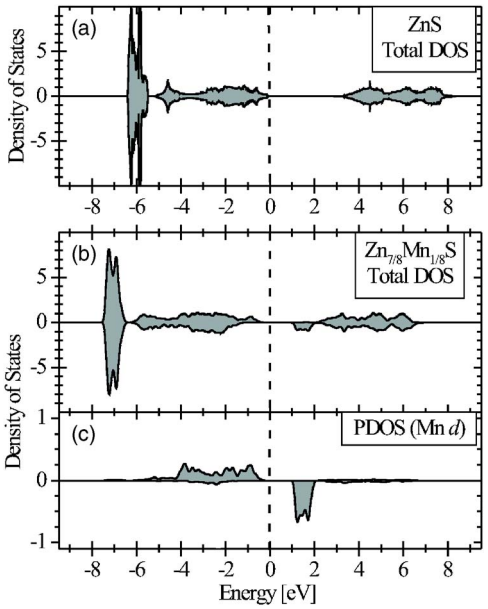

FIG. 1. Total density of states comparison of pure ZnS in the zinc-blende structure (a) and the substitutionally doped DMS $Zn_{0.875}Mn_{0.125}S$ in the wurtzite structure (b). The Fermi energy is set to zero, positive DOS values correspond to spin-majority states, and negative DOS values correspond to spin-minority states. The inclusion of Mn d states near the Fermi energy [shown independently in the partial density of states of plot (c)] significantly alters the magnitude and character of the energy gap between occupied and unoccupied electronic states.

While the XRD measurements have shown our experimental crystal to have wurtzite structure, a doping level of 10% in ZnS has been described as a boundary doping level between a sample having wurtzite or zinc-blende structure, with concentrations less than or equal to 10% resulting in zinc-blende crystals and greater than 10% resulting in wurtzite crystals.[3] With this fact in mind, DFT calculations have also been performed using a zinc-blende crystal structure for our 10% doped sample, with little variation noted between the DOS for the different crystal structures.[37]

RESULTS

Upon comparison of the total densities of states calculations shown in Fig. 1 which display the electronic structure near $\boldsymbol{E_F}$ (0 eV) as the sum of all states for ZnS (a) and doped $Zn_{0.875}Mn_{0.125}S$ (b), we see that a number of features develop with the introduction of Mn defect states [shown in Fig. 1(c)] to the ZnS crystal lattice. In the valence band, the introduction of a weak enhancement of valence spin-majority states located 0–0.5 eV below $\boldsymbol{E_F}$, attributed to Mn $3d$ localized states, shifts the general Zn s, Zn d, and S p features remain-

ing within the valence band to lower energies relative to $\boldsymbol{E_F}$. The opposite effect occurs above $\boldsymbol{E_F}$, where Mn $3d$ states in the conduction band of $Zn_{11}MnS_{12}$ appear at lower energies (+2.0 eV) than the initial conduction states in ZnS (+3.0 eV) pulling the other conduction-band states slightly closer to the Fermi edge. The overall effect of these changes is to shrink the energy gap between valence and conduction states from 3.34 to 1.71 eV, with states at the top and bottom of this gap being characterized mainly as Mn d states, as shown in Fig. 1(c). We wish to note that the partial densities of states for individual components of Zn_7MnS_8 (shown in Fig. 4 and discussed later in the text) shows that the lowest energy dipole-allowed transition ($\Delta\ell = \pm 1$) between valence and conduction states would be a charge-transfer excitation between Mn d and S p states, suggesting an optical gap of approximately 3.5 eV, which is larger than the d-d conduction gap [2.2 eV in Fig. 1(c)] and comparable to previously determined band-gap magnitudes for $Zn_{1-x}Mn_xS$ (3.73 eV).[38]

The introduction of Mn atoms also creates a level of spin polarization between the majority and minority spin states that is not present in the ZnS DOS, indicating the presence of a magnetic moment in our unit cell due to the inclusion of the Mn atoms. Our DOS calculations for $Zn_{0.875}Mn_{0.125}S$ show features similar to total DOS calculations for $Zn_{0.75}Mn_{0.25}O$,[9] which also show a large density of Zn $3d$ states about 7 eV below $\boldsymbol{E_F}$ and spin-minority states at the bottom of the conduction band. However, the insulating gap in this calculation is considerably smaller than our calculated gap, which is to be expected considering the significant difference in doping levels. Valence-band information similar to that predicted in our DOS has also been obtained experimentally from photoemission measurements of $Zn_{0.81}Mn_{0.19}S$,[13] with the exception of a large presence of Mn $3d$ states 3 eV below $\boldsymbol{E_F}$ which does not appear in our DOS, most likely due to the lower concentration of Mn atoms or other computational factors.

Our x-ray absorption spectra of the Mn $L_{2,3}$-edge of the $Zn_{0.90}Mn_{0.10}S$ sample is shown in Fig. 2, compared with that of a pure Mn metal chip. The $Zn_{0.90}Mn_{0.10}S$ spectrum is a partial fluorescence yield (PFY) measurement, while the Mn metal spectra is a total electron yield (TEY) measurement. Many of the relatively small variances between the two spectra can be attributed to the differences in the data collection technique: TEY is proportional to the absorption cross section modified by the escape probability of the electron within the system, while PFY is proportional to the absorption cross section modified by self absorption and Raman scattering processes, especially near the absorption threshold. In the case of our DMS sample, PFY measurements give an improved representation of the absorption cross section over TEY because the Mn in the sample is dilute,[23,39] and the insulating nature of the sample affects the electron yield measured by TEY while not affecting the PFY measurements.

In the x-ray absorption process, the $2p$ core hole strongly affects the energy of the $3d$ states and the resulting final state energies have an atomic-like multiplet splitting. Thus when interpreting core level absorption spectra in terms of electronic ground states one is faced with the dilemma that the

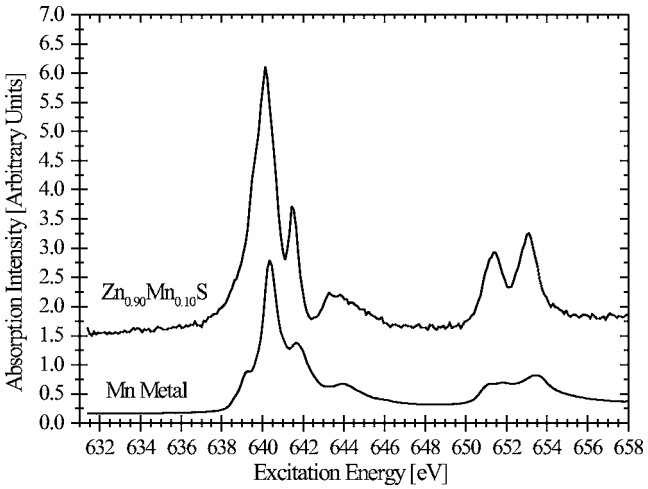

FIG. 2. Mn $L_{2,3}$-edge absorption spectra of Mn metal (TEY) and $Zn_{0.90}Mn_{0.10}S$ (PFY) samples. The Mn L_3 and L_2 edges are present in both spectra at energies of 640 and 651 eV, respectively.

delocalized $3d$ states become localized by the point-like core hole potential and thus exhibit a mixture of band-like and localized character.[40] The theoretical model of our x-ray-absorption data developed in this paper emphasizes the band-like (delocalized) character. The localized model has been addressed in a separate publication, which also extends the experimental data to other $3d$ transition-metal impurities.[23]

The general peak structures of the two absorption spectra are very similar, with the Mn L_3 ($\sim$640 eV) and L_2 ($\sim$651 eV) peaks providing the basic structure, along with various multiplet peaks resulting from dipole transitions from the $2p^6 3d^5\ ^6S$ ground state to a subset of $2p^5 3d^6$ and related final states. Thus we can state with confidence that there exist unoccupied Mn $3d$ states a few eV above the Fermi energy. The Mn metal spectra resembles previously published MnO spectra,[41] most likely owing to a small level of surface oxidation on the chip which would be detected by the surface-sensitive TEY measurements. Such oxidation is unlikely in $Zn_{0.90}Mn_{0.10}S$ and should not significantly influence the bulk-sensitive PFY measurements. The similarity between the two spectra suggests a high level of bonding between the Mn and S atoms in the sample bulk, producing an absorption spectrum similar to Mn^{2+} absorption in MnO and MnF_2.[24]

Several differences are evident in the comparison of our XES data for the $Zn_{0.90}Mn_{0.10}S$ and Mn metal samples, shown in Fig. 3. In the upper plot (a) the excitation energy used to produce the core hole and trigger the emission decay process is set at 663 eV, well above the Mn $L_{2,3}$ absorption edge. This is done to produce nonresonant x-ray emission by the electrons within the sample. As in the XAS spectra, the peaks representing transitions to the L_3 ($2p_{3/2}$) and L_2 ($2p_{1/2}$) energy levels are clearly displayed at energies of $\sim$637.5 eV and $\sim$649 eV, respectively. Comparing the two spectra, we note the appearance of a small shoulder on the low-energy side of the L_3 peak ($\sim$634 eV) as well as an energy shift of the main L_3 peak to $\sim$639 eV in the doped ZnMnS sample, resulting in an apparent spin-orbit splitting between the L_2 and L_3 peaks which is smaller than measured in the XAS

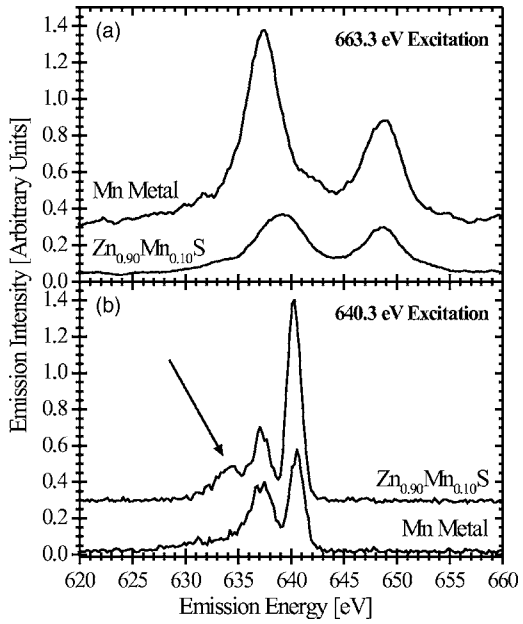

FIG. 3. Soft x-ray emission spectra comparison of $Zn_{0.90}Mn_{0.10}S$ with Mn metal, displaying nonresonant (a) and resonant (b) emission. The arrow in the lower plot indicates the presence of a second inelastic peak for Mn isolated in ZnS.

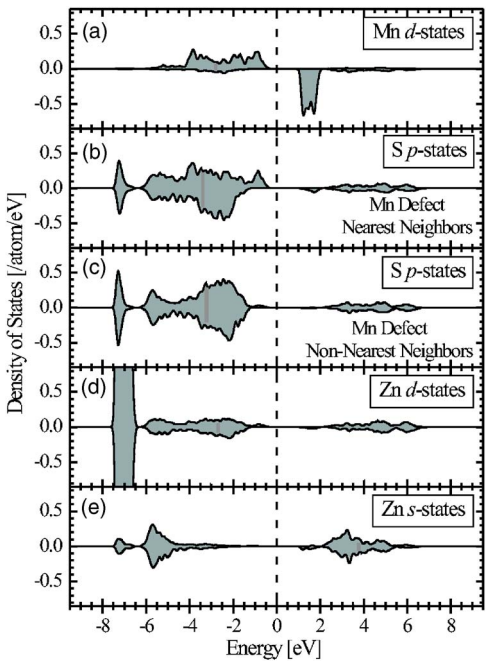

FIG. 4. Calculated partial densities of states in a theoretical $Zn_{0.875}Mn_{0.125}S$ matrix, showing Mn *d* (a), S *p* (b) and (c), Zn *d* (d), and Zn *s* (e) states. The densities of S *p* states are further divided into those that are nearest neighbors of the Mn defect (c) and those located farther away (b) in our 16-atom matrix. The Fermi energy is set to zero, positive DOS values correspond to spin-majority states, and negative DOS values correspond to spin-minority states.

spectra as well as the Mn metal XES spectrum. This observation is likely related to the mixing of Mn^{3+} with Mn^{2+} valence states, a condition which has been observed to modify the energy position and intensity of the different terms associated with the $2p^5\,{}^2P_{3/2}$ and $2p^5\,{}^2P_{1/2}$ hole states.[24]

The comparison displayed in the lower plot (b) in Fig. 3 is the XES spectra obtained with the excitation energy set at the most prominent absorption peak above the Mn L_3 absorption edge (640.3 eV), corresponding to the promotion of a $2p$ electron into a $3d$ orbit which couples with the hole to form primarily a ${}^6P$ term. The resulting relaxation of this state yields elastic and inelastic emission from the sample. The Mn metal sample and our doped $Zn_{0.90}Mn_{0.10}S$ sample show emission peaks at 640 eV (elastic recombination peak) and 637 eV (inelastic peak), but the $Zn_{0.90}Mn_{0.10}S$ sample spectra also exhibits a second inelastic peak (denoted by the arrow) at 634 eV which is not evident in the emission from the Mn metal but is seen in MnO (5 eV loss)[41] and MnF_2 (4.6 eV loss).[24]

The variations between the XES measurements of Mn metal and our $Zn_{0.90}Mn_{0.10}S$ sample appear to be due to Zn $3d$ and S $3p$ states which are largely hybridized with the Mn $3d$ states in the valence band, as displayed in the calculated partial density of states (Fig. 4) for Mn *d* (a), S *p* (b and c), Zn *d* (d), and Zn *s* (e) states. This hybridization brings about a number of valence states having *d* character that mix primarily with S *p* states at lower energies than the principle *d* states just below $\boldsymbol{E_F}$, creating the low-energy shoulder seen in the nonresonant XES spectra [Fig. 3(a)] of the $Zn_{0.90}Mn_{0.10}S$ sample while the principle Mn $3d$ emitting states are pushed to slightly higher energy as indicated by the main L_3 peak in the emission plot.

The PDOS of the S atoms shown in Fig. 4 have been divided into the contributions from the Mn atom's nearest neighbors (b) and the non-nearest neighbors (c) in order to show the range of influence exerted by the defect Mn atoms upon the S atoms. For comparison, the PDOS of the Mn and Zn *d* states are shown in panels (a) and (d), respectively. It should be noted that the sulfur PDOS plots have not been normalized to the absolute number of atoms contributing to each, and in our theoretical 24-atom crystal there are twice as many non-nearest-neighbor S atoms than nearest-neighbor S atoms. When compared to the PDOS of the S atoms in plot (c) (non-nearest-neighbor atoms), the PDOS of the nearest-neighbor S atoms show several differences, including: an increased number of S *p* states located just below the Fermi energy as well as approximately 1.5–2.0 eV above $\boldsymbol{E_F}$, an asymmetry between spin majority and spin minority states, and a larger amount of hybridization with the Mn PDOS than non-nearest-neighbor S atoms. The occupied Mn *d* states also extend into the valence band in a manner similar to that of the nearest-neighbor S *p* states between −1 and −4 eV, while at energies below −4 eV the S *p* states appear to be hybridized with the Zn *d* states and Zn *s* states, indicating *sp-d* hybridization throughout the valence band. Nonetheless, in the dilute impurity regime, which is the case considered here, the magnetic properties of the Mn atoms are not much different from the free atomic case, as evidenced by the fact that the calculated moment of the Mn ion is $5.00\mu_B$, yielding a magnetization in the calculated Zn_7MnS_8 system of 65 emu/cm^3, which is expected for a pure Mn metal. Furthermore, our calculations show that the Mn *d* states are completely spin polarized, a characteristic important for pro-

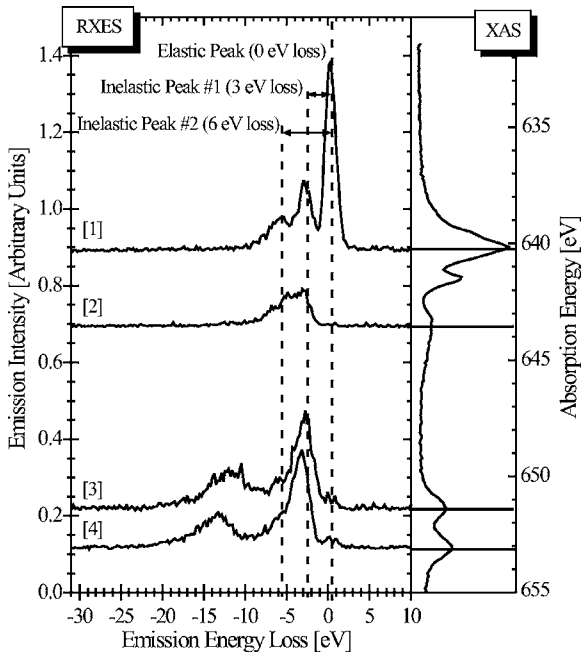

FIG. 5. RXES measurements (left) of the Mn L_3 and L_2 edges of $Zn_{0.90}Mn_{0.10}S$ performed at excitation energies as indicated on the XAS plot (right). The emission energy scale was found by subtracting the excitation energy from the true measured emission energy. In each spectrum we see an elastic peak (0-eV loss), and two inelastic peaks representing transitional energy losses of 3 and 6 eV.

ducing many of the interesting features in Mn-doped DMS.

Further evidence of localization is presented in the resonant x-ray emission spectroscopy (RXES) measurements displayed in Fig. 5, which indicate that the two inelastic peaks seen in Fig. 3(b) are evident as the excitation energy is tuned to various energy positions in the absorption spectra. Subtracting the excitation energy from the emission energy, we see the elastic peak is at nearly the same energy as the excitation energy (energy loss of 0 eV), and that the two inelastic peaks correspond to energy losses of approximately 3 and 6 eV. These results closely resemble energy loss emission spectra measured by our group[42] and separately reported by Butorin *et al.*, who measured loss features in a similar fashion at energies of 3 and 5 eV in MnO.[41] From this comparison, we determine the initial (inelastic peak 1) to be the result of a spin-flip, *d-d* electron transfer from the $2p^6 3d^5$ (^6S) ground state of the Mn atom into a localized orbital within the conduction band corresponding to the $2p^6 3d^5$ (^4G) excited state, as explained in Ref. 7 and verified by our DOS [Fig. 4(a)] which show states having primarily Mn *d* character at the top of the occupied valence band and at the bottom of the unoccupied conduction band to be separated by approximately 2.5 eV. This interpretation also works well for the lowest energy transfer in MnO,[41] and the highly ionic compound MnF_2,[24] although we note that within the band picture a transition of this type requires a 3*d* electron having spin majority symmetry at the top of the valence band to be transferred into a spin minority state in the conduction band as suggested by the isolated atom model.[23]

The appearance of the second inelastic peak corresponding to a 6-eV loss can be addressed by comparing the RXES measurements to the DOS calculations, where we see that the magnitude of energy loss for inelastic peak 2 suggests this energy loss may be due to either a charge-transfer process or an excitation of the valence electron to an excited term of the d^5 ground-state configuration. Because of the significant hybridization as displayed in the DOS (Fig. 4), it is more appropriate to discuss the transition responsible for inelastic peak 2 in terms of band structure and a charge transfer than as an electronic transfer. The most likely characterization of the 6-eV loss is that of a charge transfer, as the magnitude of this energy loss for excitation to the Mn *d* states at the bottom of the conduction band (RXES spectra [1] and [3]) places the states responsible for the transfer of an electron in a valence-band region composed mainly of S *p* states hybridized with the Mn and Zn *d* states. The Zn *s* states lie at lower energies in the valence band (−5 eV) and may also contribute to the width of this inelastic peak. Excitation to the absorption states located approximately 5.5 eV above $\boldsymbol{E_F}$ (RXES spectra [2]), a conduction-band region which is composed primarily of states characterized as S *p* and Zn *s* with a small level of Mn *d* states as shown in the PDOS of Figs. 4(c) and 4(e), places the emitting valence states as the Mn *d* states at the top of the valence band. In each of the cases described above, we encounter an electron transfer between Mn sites and S or Zn atomic states hybridized throughout both the valence and conduction bands. Further comparison with MnO measurements show a similar group of satellite peaks extending over a range of more than 5 eV on the low-energy side of the spectra which are described as being produced by charge-transfer excitations resulting in a $3d^6\,\underline{L}$ state, where $\underline{L}$ denotes a ligand hole in the O 2*p* band for MnO.[41] The presence of a similar mechanism in the bonding of the Mn and S atoms in our $Zn_{0.90}Mn_{0.10}S$ sample is clearly displayed by the 6-eV energy loss of inelastic peak (2), which appears to extend over a range of 4 eV, and is thus described as resulting in a $3d^6\,\underline{L}$ final state.

The second possibility is that the 6-eV loss could be the result of a *d-d* transition between Mn *d* states, which are spread throughout the valence band (from −7 to 0 eV) and conduction band (+1.5 to +7.5 eV) due to their hybridization with the S *p* states. While such transitions likely contribute to the spectral peak, the density of Mn *d* states below −0.5 eV is considerably lower than that of the S *p* states, implying the dominant character of this region to be that of S *p*. The presence of Zn *d* states at these energies also provides the possibility of a *d-d* transition between Zn and Mn elements, although if Zn-Mn transitions were being measured, we would expect to see a rather intense energy-loss feature of approximately 8.5 eV, owing to the large Zn *d* PDOS located 6.5 eV below $\boldsymbol{E_F}$.

The presence of significant *pd* hybridization at the top of the valence band is of considerable importance for the practical possibilities of DMS materials. The dipole approximation for optical transitions rules out electron excitation between the Hubbard split Mn *d* bands, encouraging charge-transfer excitations between the valence S *p* states and conduction Mn *d* states. The much smaller contribution of S *p* states at the bottom of the conduction band suggests a much lower probability of a similar transition from valence Mn *d* states to conduction S *p* states. However, magnetic

spin-flip transitions between the nearly completely spin-polarized valence and conduction states within the Mn atoms are allowed and have been observed in similar systems,[24,43] providing another possible degree of freedom for transitions across the energy gap. The use of Mn, with its five unpaired 3*d* electrons, as a dopant for such systems in order to provide spin polarization appears to be quite important. The effects of different dopants in ZnS compounds will be explored in a forthcoming paper.[44]

CONCLUSIONS

Our x-ray emission and absorption measurements suggest a significant level of hybridization throughout the valence and conduction bands, although it is shown to be most prevalent between Mn *d* states and S *p* states within the valence band. Used in conjunction with the calculated densities of states we can assume that Mn and S atoms play a majority role in the bonding of the Mn atoms when a ZnS sample is doped to create a diluted magnetic semiconductor. The close relationship between our x-ray measurements of $Zn_{0.90}Mn_{0.10}S$ and measurements of MnO suggest that the states near $\boldsymbol{E_F}$ of $Zn_{1-x}Mn_xS$ compounds behave mainly as if the compound was MnS, with the Zn *s* and *d* states providing relatively little influence on Mn 3*d* bonded states within 4 eV of the Fermi energy,[45] and exhibiting transition energy features in accordance with optical absorption measurements.[46] The resonant x-ray emission spectra suggest a semiconducting band gap with a magnitude of approximately 3 eV (±1.0 eV). The band gap is described as being primarily of spin-flip, *d-d* character with elements of charge-transfer character brought on by the *p-d* hybridization between the S and Mn electron states just below $\boldsymbol{E_F}$ as shown in the calculated PDOS. RXES measurements show a broad inelastic spectral peak centered at an energy loss of approximately 6 eV and appears to spread over the region between −3.5 and −7.5 eV, which we believe indicates the primary charge-transfer transition in the $Zn_{0.90}Mn_{0.10}S$ system, which is in accordance with that predicted by our density-of-states calculations.

ACKNOWLEDGMENTS

We wish to acknowledge helpful discussions with Professor J. Jiménez-Mier of Instituto de Ciencias Nucleares, UNAM, and Professor J. P. Perdew of Tulane University. The computations were supported by the awards NSF DMR-9971573, NSF/LEQSF(2001-04)-RII03, and NSF/EPS-0083046. The experiments were supported by the DOE under Contract No. DE-FG02-01ER45917. The ALS at Lawrence Berkeley National Laboratory is supported by DOE Contract No. DE-A003-76SF00098.

*Current address: Seagate Technology, Shakopee, MN 55379, USA.

†Current address: Department of Chemistry and Geochemistry, Colorado School of Mines, Golden, CO 80401, USA.

[1] H. Ohno, Science **281**, 951 (1998).

[2] *Diluted Magnetic Semiconductors, Semiconductors and Semimetals* Vol. 25, edited by J. K. Furdyna and J. Kossut (Academic Press, Boston, 1988).

[3] J. K. Furdyna, J. Appl. Phys. **64**, R29 (1988).

[4] J. K. Furdyna, J. Appl. Phys. **53**, 7637 (1982).

[5] H. Saito, V. Zayets, S. Yamagata, and K. Ando, Phys. Rev. Lett. **90**, 207202 (2003).

[6] J. A. Gaj, R. R. Galazka, and M. Nawrocki, Solid State Commun. **25**, 193 (1978).

[7] R. L. Aggarwal, S. N. Jasperson, P. Becla, and J. K. Furdyna, Phys. Rev. B **34**, 5894 (1986); Y. R. Lee, A. K. Ramdas, and R. L. Aggarwal, *ibid.* **33**, 7383 (1986).

[8] J. F. Dillon, Jr., J. K. Furdyna, U. Debska, and A. Mycielski, J. Appl. Phys. **67**, 4917 (1991).

[9] K. Sato and H. Katayama-Yoshida, Semicond. Sci. Technol. **17**, 367 (2002).

[10] J. Okabayashi, A. Kimura, O. Rader, T. Mizokawa, A. Fujimori, T. Hayashi, and M. Tanaka, Phys. Rev. B **64**, 125304 (2001).

[11] J. Okabayashi, A. Kimura, T. Mizokawa, A. Fujimori, T. Hayashi, and M. Tanaka, Phys. Rev. B **59**, R2486 (1999).

[12] E. Z. Kurmaev (private communication). V. I. Sokolov, A. N. Mamedov, V. V. Chernyaev, E. Z. Kurmaev, V. R. Galakhov, S. N. Nemnonov, V. P. Kulakov, and A. V. Fadeev, Fiz. Tverd. Tela (Leningrad) **27**, 2118 (1985).

[13] R. Weidemann, H. E. Gumlich, M. Kupsch, H. U. Middelmann, and U. Becker, Phys. Rev. B **45**, 1172 (1992).

[14] J. van Elp, R. H. Potze, H. Eskes, R. Berger, and G. A. Sawatzky, Phys. Rev. B **44**, 1530 (1991).

[15] F. J. Himpsel, Phys. Rev. Lett. **67**, 2363 (1991).

[16] R. A. Stern, T. M. Schuler, J. M. MacLaren, D. L. Ederer, V. Perez-Dieste, and F. J. Himpsel, J. Appl. Phys. **95**, 7468 (2004).

[17] D. Lang and L. Kimerling, Appl. Phys. Lett. **28**, 248 (1976).

[18] R. Matz and H. Lueth, Appl. Phys. **18**, 123 (1979).

[19] V. R. Galakhov, T. P. Surkova, M. V. Yablonskikh, A. V. Sokolov, E. Z. Kurmaev, L. Gridneva, S. Bartkowski, M. Neumann, J. Nordgren, and S. A. Lopez-Rivera, Phys. Rev. B **68**, 033204 (2003).

[20] J. Okabayashi, A. Kimura, O. Rader, T. Mizokawa, A. Fujimori, T. Hayashi, and M. Tanaka, Phys. Rev. B **58**, R4211 (1998).

[21] S. Jimenez-Sandoval, A. Lopez-Rivera, and J. C. Irwin, Phys. Rev. B **68**, 054303 (2003).

[22] P. H. Keesom, Phys. Rev. B **33**, 6512 (1986).

[23] V. Perez-Dieste, J. N. Crain, A. Kirakosian, J. L. McChesney, E. Arenholz, A. T. Young, J. D. Denlinger, D. L. Ederer, T. A. Callcott, S. A. Lopez-Rivera, and F. J. Himpsel, Phys. Rev. B **70**, 085205 (2004).

[24] J. Jiménez-Mier, D. L. Ederer, and T. Schuler, Phys. Rev. A **68**, 042715 (2003); Phys. Rev. B **70**, 035216 (2004).

[25] S. A. Lopez-Rivera (unpublished).

[26] D. R. Yoder-Short, U. Debska, and J. K. Furdyna, J. Appl. Phys. **58**, 4056 (1985).

[27] Y. L. Soo, Z. H. Ming, S. W. Huang, Y. H. Kao, R. N. Bhargava, and D. Gallagher, Phys. Rev. B **50**, 7602 (1994).

[28] J. J. Jia, T. A. Calcott, J. Yurkas, A. W. Ellis, F. J. Himpsel, M. G. Samant, J. Stohr, D. L. Ederer, J. A. Carlisle, E. A. Hudson, L. J. Terminello, D. K. Shuh, and R. C. C. Perera, Rev. Sci. Instrum. **66**, 1394 (1995).

[29] J. A. Bearden, Rev. Mod. Phys. **39**, 78 (1967); J. A. Bearden and A. F. Burr, *ibid.* **39**, 125 (1967); Richard D. Deslattes, Ernest G. Kessler, Jr., P. Indelicato, L. de Billy, E. Lindroth, and J. Anton, *ibid.* **75**, 35 (2003).

[30] DFT calculations performed by R. McNorton, R. A. Stern, S. D. Willoughby, and J. M. MacLaren.

[31] G. Kresse and J. Furthmuller, Vienna Ab-Initio Simulation Package (2001), http://cms.mpi.univie.ac.at/vasp/

[32] P. E. Blochl, Phys. Rev. B **50**, 17953 (1994).

[33] G. Kresse and D. Joubert, Phys. Rev. B **59**, 1758 (1999).

[34] J. P. Perdew, K. Burke, and M. Ernzerhof, Phys. Rev. Lett. **77**, 3865 (1996).

[35] J. P. Perdew, in *Electronic Structure of Solids '91*, 1st edition, edited by P. Ziesche and H. Eschrig (Akademie, Berlin, 1991).

[36] S. H. Vosko, L. Wilk, and M. Nusair, Can. J. Phys. **58**, 1200 (1980).

[37] R. McNorton, T. M. Schuler, R. A. Stern, J. M. MacLaren, and D. L. Ederer (unpublished).

[38] R. N. Bhargava, D. Gallagher, X. Hong, and A. Nurmikko, Phys. Rev. Lett. **72**, 416 (1994); V. Albe, C. Jouanin, and D. Bertho, Phys. Rev. B **57**, 8778 (1998).

[39] J. Jaklevic, J. A. Kirby, M. P. Klein, A. S. Robertson, G. S. Brown, and P. Eisenberger, Solid State Commun. **88**, 679 (1977).

[40] G. van der Laan and I. W. Kirkman, J. Phys.: Condens. Matter **4**, 4189 (1992).

[41] S. M. Butorin, J. H. Guo, M. Magnuson, P. Kuiper, and J. Nordgren, Phys. Rev. B **54**, 4405 (1996).

[42] T. M. Schuler, J. Jiménez-Mier, and D. L. Ederer (unpublished).

[43] L. Braicovich, C. Dallera, G. Ghiringhelli, N. B. Brookes, J. B. Goedkoop, and M. A. van Veenendaal, Phys. Rev. B **55**, R15989 (1997).

[44] R. McNorton, R. A. Stern, T. M. Schuler, J. M. MacLaren, D. L. Ederer, D. A. Resnick, K. Gilmore, Y. U. Idzerda, V. Perez-Dieste, F. J. Himpsel, S. A. Lopez-Rivera, and T. A. Callcott (unpublished).

[45] H. Sato, T. Mihara, A. Furuta, M. Tamura, K. Mimura, N. Happo, M. Taniguchi, and Y. Ueda, Phys. Rev. B **56**, 7222 (1997).

[46] D. R. Huffman and R. L. Wild, Phys. Rev. **156**, 989 (1967).